

Constraints on sterile neutrinos and the cosmological tensions

Supriya Pan,^{1,2,*} Osamu Seto,^{3,†} Tomo Takahashi,^{4,‡} and Yo Toda^{3,§}

¹*Department of Mathematics, Presidency University, Kolkata 700073, India*

²*Institute of Systems Science, Durban University of Technology,
PO Box 1334, Durban 4000, Republic of South Africa*

³*Department of Physics, Hokkaido University, Sapporo 060-0810, Japan*

⁴*Department of Physics, Saga University, Saga 840-8502, Japan*

Abstract

We investigate cosmological bounds on sterile neutrino masses in the light of the Hubble and S_8 tensions. We argue that nonzero masses for sterile neutrinos are inferred at 2σ level in some extended models such as varying dark energy equation of state, when a direct measurement of the Hubble constant H_0 and weak lensing measurement of dark energy survey (DES) are taken into account. Furthermore, the Hubble and S_8 tensions are also reduced in such a framework. We also consider the case where a nonflat Universe is allowed and show that a slightly open Universe may be favored in models with sterile neutrinos in the context of the cosmological tensions.

* supriya.maths@presiuniv.ac.in

† seto@particle.sci.hokudai.ac.jp

‡ tomot@cc.saga-u.ac.jp

§ y-toda@particle.sci.hokudai.ac.jp

I. INTRODUCTION

The large scale properties of our Universe are well described by the standard Λ -cold dark matter (Λ CDM) cosmological model, where the cosmological constant Λ plays a role of dark energy whose equation of state (EoS) parameter w corresponds to -1 . Although the Λ CDM model has been extremely successful in explaining the large scale structure of the Universe, however, there are several tensions between different measurements. One of the most serious issues which has been discussed much recently is the discrepancy of the Hubble constant H_0 between indirect and local direct measurements. The Planck measurement of the cosmic microwave background (CMB), the prime indirect measurements of H_0 , infers $H_0 = (67.4 \pm 0.5)$ km/sec/Mpc at 68% C.L. [1], on the other hand, local direct measurements of H_0 , such as those made using a distance ladder and strong gravitational lensing observations, consistently yield a value higher than that obtained from CMB (e.g., [2–6]). For example, the Cepheid-supernovae distance ladder provides $H_0 = 73.04 \pm 1.04$ km/sec/Mpc [2]. For reviews on the Hubble constant tension, see e.g., Refs. [7–12]. Another tension is in the value of the amplitude of matter fluctuations, σ_8 , at the scale of 8 Mpc/ h , which is sometime recast as the S_8 parameter defined by $S_8 = \sigma_8 \sqrt{\Omega_m/0.3}$. The inferred value of S_8 from CMB by Planck [1] is larger than those measured by low red-shift probes through weak gravitational lensing and galaxy clustering [13–20].

Motivated by the issues mentioned above, it is worth investigating cosmological models beyond Λ CDM. Although some simple extensions have been studied in the Planck 2018 paper [1], such simple extended models cannot address the discrepancies. In particular, even when we only consider the data from Planck, they cannot simultaneously increase H_0 and decrease σ_8 , which can be summarized as follows. As the sum of neutrino mass $\sum m_\nu$ increases, both H_0 and σ_8 decrease. As the curvature density parameter Ω_K decreases, both H_0 and σ_8 decrease for CMB data only, while it becomes consistent with a flat Universe when we include baryon acoustic oscillation (BAO) data. As the effective number of neutrino species N_{eff} increases, both H_0 and σ_8 increase although eventually becomes consistent with the prediction of the standard model of particle physics and the Large Electron Positron Collider (LEP) results indicating three generations of neutrinos [21]. It should also be noted that none of these models cannot explain even a single tension when the combination of CMB and BAO data is adopted in the analysis.

Although three generations of neutrinos with nonvanishing masses and mixings explain various neutrino oscillation phenomena well in general, by examining each experiment in detail, it appears that there are multiple tensions between them. In addition, the best-fit value of the mass squared difference for IceCube data is given as $\Delta m^2 \sim 4 \text{ eV}^2$ [22] even though the data is consistent with no sterile neutrino. Furthermore, measurements of Δm_{12}^2 by the Super Kamiokande [23] and the KamLAND [24] also show mild discrepancy between them. Consequently, sterile neutrinos remain phenomenologically motivated (see for instance [25–32]), despite that sterile neutrinos are challenged in other neutrino experiments [33–35] and cosmological data [1, 36].

Cosmological constraints on such an eV mass sterile neutrino mostly come from CMB, big bang nucleosynthesis (BBN), and structure formation through the increase of N_{eff} and its free-streaming effect. Since right after the LSND results were published, incompatibility of such sterile neutrinos with BBN due to thermalization of sterile neutrino and the resultant large N_{eff} has been pointed out [37–39]. However, by introducing large lepton asymmetry of $\mathcal{O}(10^{-2})$, which is permissible by current cosmological observations [40], one can relax the BBN constraint [36, 41]. A general equation of state (EoS) of dark energy [42] or an $f(R)$ theory of gravity [43] could also eliminate the constraint on free streaming, which may still allow the sterile neutrinos.

As is well known, just introducing sterile neutrinos is not favored by the cosmological observations and it makes the fitting worse. Thus, we introduce an additional ingredient to sterile neutrinos which might counteract or dominate over the effects from sterile neutrinos. As such an additional constituent, we consider the spatial curvature of the Universe, which may be somewhat motivated as it has been argued that CMB lensing magnitude indicates nonzero positive spatial curvature at several standard deviations [1, 44, 45]. Another motivation might be that, in order that the varying electron mass can work as a solution to the Hubble tension [46], which is regarded as so far one of the best models to resolve the tension [9], a positive spatial curvature would be preferable. This model is still consistent with BBN although the BBN data slightly prefers no variation of electron mass [47]. Furthermore, it is interesting to note that larger neutrino masses are allowed in this framework [48].

Another simple extension is to consider some time-varying dark energy EoS rather than assuming a cosmological constant as dark energy. Although a simple time variation in

the dark energy EoS such as the Chevallier-Polarski-Linder (CPL) parametrization [49, 50] would not work as a solution to the Hubble tension, another EoS model may relax it (e.g., [51]). Varying EoS (also assuming a constant EoS) may give a better fit in models with sterile neutrinos [36].

In this paper, the fit of cosmological models with sterile neutrinos is examined, incorporating either the spatial curvature or assuming the CPL parametrization for dark energy EoS. We perform our analysis for two different datasets: one set consists of CMB, BAO, and type Ia supernovae (SNeIa) while the other set additionally includes the SH0ES (Supernovae and H_0 for the EoS of dark energy) [2] (which is referred to as “R21” hereafter) and Dark Energy Survey (DES) data [52], which give inconsistent values for H_0 and $\sigma_8(S_8)$, respectively. When we include R21 and DES, we show, by introducing additional parameters of the spatial curvature or the dark energy, a cosmological model with sterile neutrinos appears to indicate larger H_0 and smaller σ_8 (S_8) simultaneously. We also find that a slightly negative curvature (open) Universe is favored when we consider a nonflat Universe and eV-scale sterile neutrino mass is favored for a model with the CPL parametrization for the dark energy EoS.

This paper is organized as follows. In the next section, we summarize the method of our statistical analysis and the model framework beyond Λ CDM that we consider in this paper. In Section. III, we present our results. Section IV is devoted to conclusion.

II. MODELS, OBSERVATIONAL DATA AND METHODOLOGY

In this section, first we describe cosmological models to be analyzed to evaluate a possible contribution of sterile neutrinos. Then we give the methodology of our analysis and the data adopted in this paper to derive constraints on cosmological parameters. Bounds on cosmological parameters will be presented in the next section.

A. Models to be analyzed

1. Λ CDM: The base cosmological model which we use as the reference model to compare with other ones is the standard Λ CDM model with just six free parameters: the baryon density $\omega_b = \Omega_b h^2$, the CDM density $\omega_c = \Omega_c h^2$, the amplitude and its spectral index of

the primordial density perturbation, namely, A_s and n_s respectively, the acoustic scale $\theta_* = r_*/D_M$ with r_* the sound horizon at recombination and D_M the angular diameter distance to the last scattering surface, and the optical depth of the reionization τ .

2. Λ CDM+sterile neutrinos (labeled as “Sterile”): To implement the contribution of sterile neutrino, we include and vary the effective number of neutrinos N_{eff} and the effective mass of the sterile neutrino $m_{\nu,\text{sterile}}^{\text{eff}} = (\Delta N_{\text{eff}})^{3/4} m_{\nu,\text{sterile}}^{\text{thermal}}$ (in eV unit), as in [53]. Note that the temperature fraction is given by $(T_S/T_\nu)^3 = (\Delta N_{\text{eff}})^{3/4}$ and the density parameter of sterile neutrino is given by $\omega_{\nu,\text{sterile}} = m_{\nu,\text{sterile}}^{\text{eff}}/(94.1\text{eV})$. Here, $\Delta N_{\text{eff}} = N_{\text{eff}} - N_{\text{SM}}$ with the effective number of neutrinos in the standard model (SM) $N_{\text{SM}} = 3.046$, and $m_{\nu,\text{sterile}}^{\text{thermal}}$ is the physical mass for thermally produced sterile neutrinos.
3. $\Omega_K\Lambda$ CDM+sterile neutrinos (labeled as “ Ω_K Sterile”): We consider an extension of Λ CDM+sterile neutrinos model by allowing the curvature of the Universe to be varied by adding the curvature parameter $\omega_K = \Omega_K h^2$ in the analysis.
4. w CDM+sterile neutrinos (labeled as “ w Sterile”): Another extension of Λ CDM+sterile neutrinos model we consider is w CDM model in which the EoS of the dark energy w is considered to be a free-to-vary parameter in an interval with w being constant.
5. ww_a CDM+sterile neutrinos (labeled as “ ww_a Sterile”): Yet another extension of Λ CDM+sterile neutrinos model is to assume a time-dependent EoS (the CPL parametrization [49, 50]) which is written as

$$w(a) = w + w_a \left(1 - \frac{a}{a_0}\right) = w + \frac{z}{1+z} w_a, \quad (1)$$

where a_0 is the present value of the scale factor a , and w and $w_a = dw/da$, are respectively the dark energy EoS at the present time and its derivative with respect to the scale factor.

B. datasets and methodology

The observational datasets employed in this work are the following:

1. CMB data from Planck 2018 [54] (i.e. Planck TTTEEE+lowE) with CMB lensing [55].

Parameter	$\Omega_b h^2$	$\Omega_c h^2$	τ	n_s	$\ln(10^{10} A_s)$	θ_*
Prior	[0.005, 0.1]	[0.001, 0.99]	[0.01, 0.8]	[0.8, 1.2]	[1.61, 3.91]	[0.5, 10]

Parameter	N_{eff}	$m_{\nu, \text{sterile}}^{\text{eff}}$	Ω_K	w	w_a
Prior	[3.0461, 4]	[0, 10]	[-0.3, 0.3]	[-2, 0]	[-2, 1]

Table I: Cosmological parameters and the prior range adopted in the analysis. We assume a flat prior for all the parameters.

2. BAO distance measurements from various galaxy surveys [56–58].
3. Local measurements of light curves and luminosity distance of type Ia supernovae, namely, the Pantheon sample [59].
4. A prior on the Hubble constant ($H_0 = 73.30 \pm 1.04$ km/sec/Mpc at 68% CL) from the SH0ES collaboration [2].
5. Weak lensing measurement from the DES Year 1 data [52, 60]. We use the data from cosmic shear and galaxy clustering + galaxy-galaxy lensing.

In all analysis, we include the data from CMB (Planck), BAO and SNeIa (Pantheon), which we denote “default” dataset in our analysis. To constrain the parameters in the cosmological scenarios described above, we perform a Markov Chain Monte Carlo (MCMC) analysis by using CosmoMC [61] which is equipped with the Gelman-Rubin convergence diagnostic [62]. We assume flat priors on all the parameters used in the MCMC analyses as shown in Table I. In particular, we note that the sterile neutrino mass is restricted to $m_{\nu, \text{sterile}}^{\text{thermal}} < 10$ eV, following the analysis done in Planck 2018 [1].

III. RESULTS

In Tables II, III, and IV, we summarize the constraints on the primary and derived parameters of the flat Λ CDM, Λ CDM+sterile neutrinos (Sterile), $\Omega_K \Lambda$ CDM+sterile neutrinos (Ω_K Sterile), w CDM+sterile neutrinos (w Sterile) and ww_a CDM+sterile neutrinos (ww_a Sterile) for various datasets treating \mathcal{D} (\equiv CMB+BAO) as the base dataset and its combination with Pantheon, DES, R21 prior. While considering Pantheon, we have not used

ΛCDM				
Parameter	\mathcal{D} +Pantheon	\mathcal{D} +R21	\mathcal{D} +Pantheon+DES	\mathcal{D} +R21+DES
$\Omega_b h^2$	0.02244 ± 0.00013	0.02259 ± 0.00013	0.02252 ± 0.00013	0.02265 ± 0.00013
$\Omega_c h^2$	0.11918 ± 0.00094	0.11765 ± 0.00088	0.11807 ± 0.00084	0.11669 ± 0.00082
$100\theta_{MC}$	1.04103 ± 0.00028	1.04126 ± 0.00029	1.04111 ± 0.00029	1.04132 ± 0.00029
τ	$0.0562^{+0.0068}_{-0.0079}$	$0.0613^{+0.0069}_{-0.0082}$	$0.0572^{+0.0068}_{-0.0084}$	$0.0580^{+0.0071}_{-0.0083}$
$\ln(10^{10} A_s)$	$3.047^{+0.013}_{-0.016}$	$3.054^{+0.014}_{-0.016}$	$3.046^{+0.013}_{-0.017}$	$3.044^{+0.015}_{-0.017}$
n_s	0.9670 ± 0.0038	0.9710 ± 0.0036	0.9692 ± 0.0036	0.9729 ± 0.0036
H_0	67.74 ± 0.42	68.49 ± 0.40	68.23 ± 0.38	68.90 ± 0.38
S_8	$0.8234^{+0.0098}_{-0.011}$	0.8090 ± 0.0099	0.8108 ± 0.0091	0.795 ± 0.010
Sterile				
Parameter	\mathcal{D} +Pantheon	\mathcal{D} +R21	\mathcal{D} +Pantheon+DES	\mathcal{D} +R21+DES
$\Omega_b h^2$	0.02249 ± 0.00014	0.02282 ± 0.00016	0.02256 ± 0.00014	0.02286 ± 0.00015
$\Omega_c h^2$	$0.1189^{+0.0033}_{-0.0022}$	$0.1245^{+0.0031}_{-0.0025}$	$0.1170^{+0.0025}_{-0.0020}$	$0.1223^{+0.0030}_{-0.0022}$
$100\theta_{MC}$	1.04091 ± 0.00033	1.04048 ± 0.00041	1.04105 ± 0.00030	1.04068 ± 0.00040
τ	0.0580 ± 0.0071	$0.0615^{+0.0071}_{-0.0084}$	$0.0588^{+0.0069}_{-0.0080}$	$0.0588^{+0.0075}_{-0.0086}$
$\ln(10^{10} A_s)$	3.053 ± 0.015	3.071 ± 0.016	$3.052^{+0.014}_{-0.016}$	3.059 ± 0.017
n_s	$0.9688^{+0.0041}_{-0.0054}$	$0.9832^{+0.0060}_{-0.0052}$	$0.9685^{+0.0039}_{-0.0047}$	$0.9835^{+0.0062}_{-0.0052}$
N_{eff}	< 3.13	$3.46^{+0.16}_{-0.14}$	$3.118^{+0.015}_{-0.059}$	$3.40^{+0.16}_{-0.13}$
$m_{\nu, \text{sterile}}^{\text{eff}}$	< 0.194	< 0.0379	$0.29^{+0.10}_{-0.25}$	< 0.0760
H_0	$67.89^{+0.40}_{-0.69}$	$70.49^{+0.94}_{-0.81}$	$67.98^{+0.40}_{-0.51}$	$70.46^{+0.98}_{-0.79}$
S_8	$0.812^{+0.019}_{-0.014}$	$0.820^{+0.014}_{-0.011}$	0.790 ± 0.015	$0.798^{+0.015}_{-0.012}$

Table II: Marginalized values and 68% confidence regions for cosmological parameters obtained combining Planck and BAO with and without other datasets (e.g. Pantheon, R21, DES), for ΛCDM model and Sterile model. Here “ \mathcal{D} ” means the combined dataset with Planck and BAO.

the R21 prior in order to avoid the twice-counting of a few hundred SNeIa [63]. Triangle plots of the marginalized posterior distributions and two dimensional joint contours of 68% and 95% C.L. are displayed in Fig. 1 (for Sterile); Figs. 2 and 3 (for Ω_K Sterile); Figs. 4 and

$\Omega_K \text{Sterile}$				
Parameter	$\mathcal{D}+\text{Pantheon}$	$\mathcal{D}+\text{R21}$	$\mathcal{D}+\text{Pantheon}+\text{DES}$	$\mathcal{D}+\text{R21}+\text{DES}$
$\Omega_b h^2$	$0.02247^{+0.00016}_{-0.00017}$	0.02261 ± 0.00021	0.02249 ± 0.00016	$0.02256^{+0.00017}_{-0.00019}$
$\Omega_c h^2$	$0.1195^{+0.0033}_{-0.0024}$	0.1238 ± 0.0029	$0.1185^{+0.0027}_{-0.0022}$	0.1222 ± 0.0028
$100\theta_{MC}$	1.04082 ± 0.00036	1.04050 ± 0.00039	1.04087 ± 0.00034	1.04059 ± 0.00039
τ	$0.0575^{+0.0068}_{-0.0078}$	$0.0603^{+0.0069}_{-0.0086}$	$0.0585^{+0.0069}_{-0.0080}$	0.0576 ± 0.0079
$\ln(10^{10} A_s)$	3.054 ± 0.015	$3.067^{+0.015}_{-0.018}$	3.055 ± 0.015	3.058 ± 0.017
n_s	$0.9671^{+0.0049}_{-0.0066}$	0.9744 ± 0.0085	$0.9659^{+0.0049}_{-0.0057}$	$0.9702^{+0.0062}_{-0.0088}$
N_{eff}	< 3.15	$3.33^{+0.11}_{-0.20}$	$3.137^{+0.025}_{-0.073}$	$3.279^{+0.092}_{-0.17}$
$m_{\nu, \text{sterile}}^{\text{eff}}$	< 0.231	< 0.0855	$0.32^{+0.14}_{-0.20}$	$0.28^{+0.14}_{-0.20}$
Ω_K	0.0013 ± 0.0021	0.0034 ± 0.0025	$0.0024^{+0.0021}_{-0.0023}$	$0.0057^{+0.0026}_{-0.0022}$
H_0	$68.25^{+0.68}_{-0.80}$	70.40 ± 0.80	68.54 ± 0.69	$70.41^{+0.67}_{-0.76}$
S_8	$0.809^{+0.021}_{-0.014}$	$0.811^{+0.019}_{-0.011}$	0.787 ± 0.015	0.777 ± 0.018

Table III: Marginalized values and 68% confidence regions for cosmological parameters obtained combining Planck and BAO with and without other datasets (e.g. Pantheon, R21, DES), for $\Omega_K \text{Sterile}$ model.

5 (for $w \text{Sterile}$); Figs. 6, and 7 (for $ww_a \text{Sterile}$). In what follows, we report the key findings of our analyses. Throughout the article, we quantify the level of the tension between two different estimates of the cosmological parameters by using the so-called Gaussian tension, which is defined by

$$T_x \equiv \frac{|x_i - x_j|}{\sqrt{\sigma_{x_i}^2 + \sigma_{x_j}^2}}, \quad (2)$$

where x_i and x_j are the estimated values from two different data i, j with σ_{x_i} and σ_{x_u} being the 1σ errors for each dataset.

A. Sterile

The 68% marginalized allowed ranges for the cosmological parameters in $\Lambda \text{CDM} + \text{sterile}$ neutrino model are summarized in Table. II. Two dimensional allowed regions and one dimensional posterior distributions are also depicted in Fig. 1. For comparison, we also show those

w Sterile				
Parameter	\mathcal{D} +Pantheon	\mathcal{D} +R21	\mathcal{D} +pantheon+DES	\mathcal{D} +R21+DES
$\Omega_b h^2$	0.02246 ± 0.00015	$0.02246^{+0.00015}_{-0.00017}$	0.02253 ± 0.00015	0.02255 ± 0.00015
$\Omega_c h^2$	$0.1194^{+0.0031}_{-0.0018}$	$0.1209^{+0.0032}_{-0.0023}$	$0.1176^{+0.0028}_{-0.0019}$	0.1196 ± 0.0022
$100\theta_{MC}$	$1.04083^{+0.00034}_{-0.00031}$	1.04068 ± 0.00035	1.04093 ± 0.00032	1.04079 ± 0.00032
τ	0.0561 ± 0.0078	0.0549 ± 0.0079	$0.0572^{+0.0070}_{-0.0080}$	0.0545 ± 0.0080
$\ln(10^{10} A_s)$	$3.050^{+0.015}_{-0.016}$	3.051 ± 0.017	$3.051^{+0.014}_{-0.016}$	3.048 ± 0.017
n_s	$0.9672^{+0.0044}_{-0.0055}$	$0.9666^{+0.0048}_{-0.0067}$	$0.9672^{+0.0043}_{-0.0050}$	$0.9668^{+0.0047}_{-0.0058}$
N_{eff}	$3.132^{+0.014}_{-0.085}$	$3.192^{+0.039}_{-0.14}$	$3.140^{+0.023}_{-0.076}$	$3.216^{+0.061}_{-0.10}$
$m_{\nu, \text{sterile}}^{\text{eff}}$	< 0.236	< 0.326	$0.35^{+0.14}_{-0.23}$	0.43 ± 0.17
w	-1.041 ± 0.035	-1.175 ± 0.049	$-1.044^{+0.037}_{-0.032}$	-1.182 ± 0.045
H_0	68.75 ± 0.92	72.29 ± 0.93	$68.89^{+0.82}_{-0.92}$	72.44 ± 0.93
S_8	$0.810^{+0.021}_{-0.013}$	$0.800^{+0.030}_{-0.020}$	0.787 ± 0.015	0.771 ± 0.017
ww_a Sterile				
Parameter	\mathcal{D} +Pantheon	\mathcal{D} +R21	\mathcal{D} +Pantheon+DES	\mathcal{D} +R21+DES
$\Omega_b h^2$	0.02244 ± 0.00015	0.02246 ± 0.00016	0.02252 ± 0.00015	0.02254 ± 0.00015
$\Omega_c h^2$	$0.1199^{+0.0032}_{-0.0020}$	$0.1210^{+0.0031}_{-0.0024}$	$0.1189^{+0.0028}_{-0.0021}$	0.1198 ± 0.0025
$100\theta_{MC}$	$1.04076^{+0.00035}_{-0.00031}$	$1.04068^{+0.00036}_{-0.00033}$	1.04081 ± 0.00033	1.04076 ± 0.00033
τ	0.0542 ± 0.0074	$0.0546^{+0.0074}_{-0.0082}$	0.0555 ± 0.0076	0.0545 ± 0.0079
$\ln(10^{10} A_s)$	3.047 ± 0.015	$3.050^{+0.016}_{-0.018}$	3.049 ± 0.016	3.049 ± 0.017
n_s	$0.9663^{+0.0044}_{-0.0055}$	$0.9663^{+0.0050}_{-0.0067}$	$0.9663^{+0.0044}_{-0.0052}$	$0.9666^{+0.0047}_{-0.0059}$
N_{eff}	$3.151^{+0.025}_{-0.10}$	$3.190^{+0.039}_{-0.14}$	$3.183^{+0.043}_{-0.11}$	$3.229^{+0.065}_{-0.12}$
$m_{\nu, \text{sterile}}^{\text{eff}}$	< 0.318	< 0.330	$0.40^{+0.16}_{-0.20}$	0.45 ± 0.18
w	-0.939 ± 0.085	$-1.19^{+0.12}_{-0.15}$	$-0.925^{+0.079}_{-0.090}$	$-1.15^{+0.12}_{-0.14}$
w_a	$-0.46^{+0.40}_{-0.31}$	$0.03^{+0.57}_{-0.38}$	$-0.56^{+0.43}_{-0.31}$	$-0.15^{+0.58}_{-0.41}$
H_0	$68.76^{+0.84}_{-0.93}$	72.35 ± 0.99	69.02 ± 0.89	72.39 ± 0.98
S_8	$0.809^{+0.022}_{-0.016}$	$0.799^{+0.028}_{-0.021}$	0.787 ± 0.015	0.771 ± 0.017

Table IV: Marginalized values and 68% confidence regions for the cosmological parameters obtained combining Planck and BAO with and without other datasets (e.g. Pantheon, R21, DES), for “ w Sterile” and “ ww_a Sterile” models.

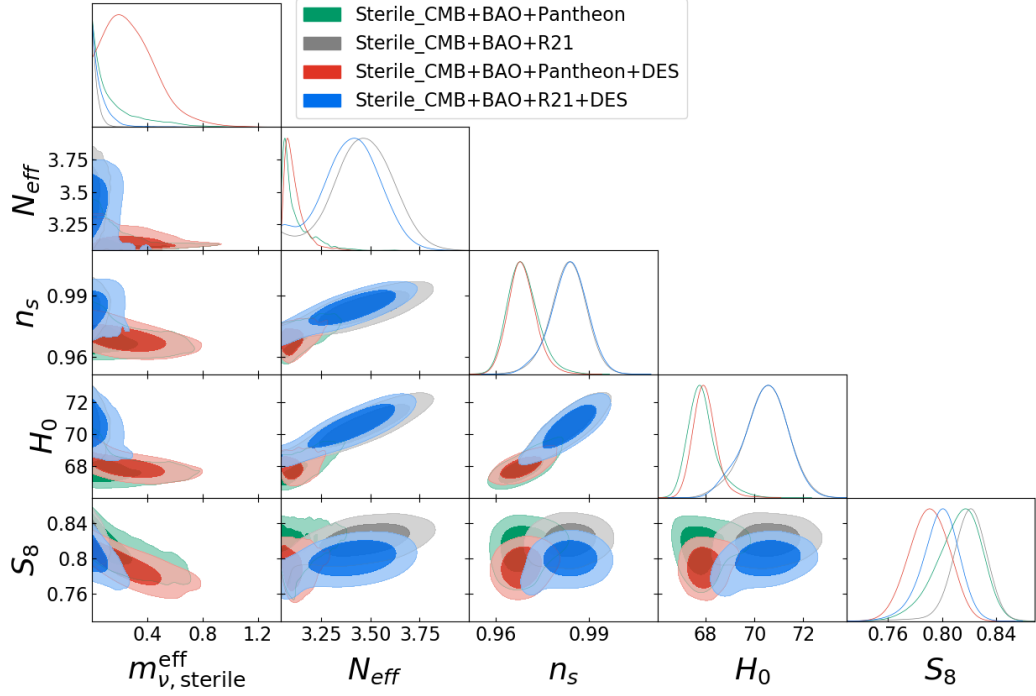


Figure 1: Posterior distributions of some parameters for the “Sterile” model. Different colors of greenish, grayish, reddish and bluish contours stand for different datasets.

in the standard Λ CDM model. As mentioned above, sterile neutrinos are parameterized by N_{eff} and $m_{\nu, \text{sterile}}^{\text{eff}}$. Interestingly, we obtained a 2σ lower bound on $m_{\nu, \text{sterile}}^{\text{eff}}$ for the combined dataset $\mathcal{D}+\text{Pantheon}+\text{DES}$. This is because as the mass of the sterile neutrino increases, the growth of matter fluctuations with a wave number greater than the free-streaming wave number $k_{\text{fs}} = 0.01(m_{\nu_s}/\text{eV})^{1/2} \text{ Mpc}^{-1}$, is suppressed [64], and it would be consistent with DES favoring low σ_8 . When we analyze the model including R21 prior and DES data (i.e. for the combined dataset $\mathcal{D}+\text{R21}+\text{DES}$), the bound on N_{eff} is given as $3.2 \lesssim N_{\text{eff}} \lesssim 3.5$, which shows almost the same tendency as the one for the case with $\Lambda\text{CDM}+N_{\text{eff}}$ model reported in the Planck paper [1]¹. This indicates that the DES data does not affect the bound on N_{eff} even in the $\Lambda\text{CDM}+\text{sterile neutrino}$ case. When the dataset of $\mathcal{D}+\text{Pantheon}+\text{DES}$ is considered, the value of S_8 is slightly decreased by including sterile neutrinos, which is also observed when usual massive neutrinos is considered [52].

¹ If we include the BBN constraint in the prior, the favored range of N_{eff} is somewhat decreased [65].

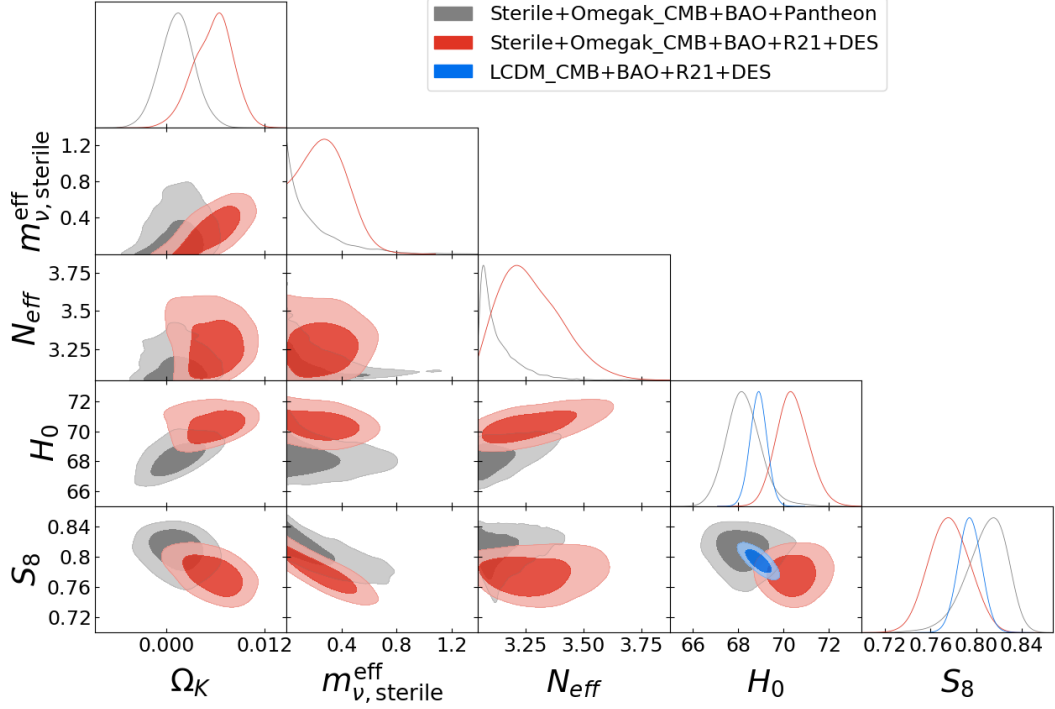


Figure 2: Posterior distributions of some parameters for “ Ω_K Sterile” model. Different colors of grayish and reddish contours stand for different datasets. For comparison, that of Λ CDM model is also shown with bluish contour.

B. Ω_K Sterile

The 68% marginalized allowed ranges for the cosmological parameters in Ω_K Sterile model are summarized in Table. III. Two dimensional allowed regions and one dimensional posterior distributions are also depicted respectively in Figs. 2 and 3 for the analysis including the R21 prior and the DES data simultaneously and separately. When we vary Ω_K in models with sterile neutrino characterized with the parameters N_{eff} and $m_{\nu,\text{sterile}}^{\text{eff}}$, a spatially flat Universe $K = 0$ is still consistent for datasets without the R21 prior and the DES data. On the other hand, when we include the R21 prior and DES data, the favored range of $3.1 \lesssim N_{\text{eff}} \lesssim 3.3$ (1σ) is obtained. Furthermore, in Ω_K Sterile model, a spatially open Universe is favored at more than 2σ and the mean value of S_8 coincides with that reported by DES.

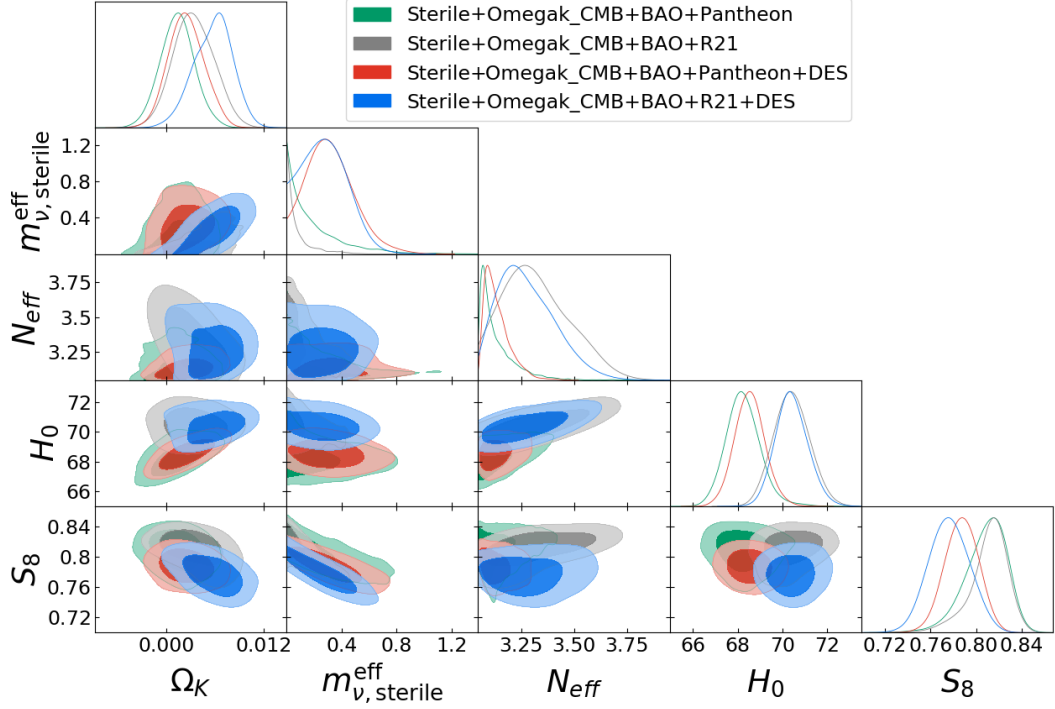


Figure 3: Posterior distributions of some parameters for “ Ω_K Sterile” model. Different colors of greenish, grayish, reddish and bluish contours stand for different datasets.

C. w Sterile

The 68% marginalized allowed ranges for the cosmological parameters of the Sterile+ w DE model are summarized in Table IV. Also the two dimensional allowed regions and one dimensional posterior distributions are shown in Figs. 4 and 5 respectively for the analysis including the R21 prior and the DES data simultaneously and separately. Indeed, a phantom dark energy ($w < -1$) is allowed for all the datasets. In particular, the evidence of $w < -1$ is strengthened in the presence of the R21 prior, i.e. for both the datasets, namely, $\mathcal{D}+\mathbf{R21}$ and $\mathcal{D}+\mathbf{R21}+\mathbf{DES}$. Moreover, when the DES data is included, a nonzero sterile neutrino mass of the order of sub-eV is found ($m_{\nu,\text{sterile}}^{\text{effective}} = 0.35^{+0.14}_{-0.23}$ at 68% CL for $\mathcal{D}+\mathbf{Pantheon}+\mathbf{DES}$). The evidence of a nonzero sterile neutrino mass is also found even for the dataset of $\mathcal{D}+\mathbf{R21}+\mathbf{DES}$. Regarding the H_0 and S_8 , we observe that in this extended scenario where w has been considered instead of Ω_K , the constraints on S_8 are almost identical with those obtained in the Ω_K Sterile scenario, however, H_0 is slightly increased (~ 2 km/sec/Mpc) in the w Sterile case only for the combined datasets $\mathcal{D}+\mathbf{R21}$ and $\mathcal{D}+\mathbf{R21}+\mathbf{DES}$.

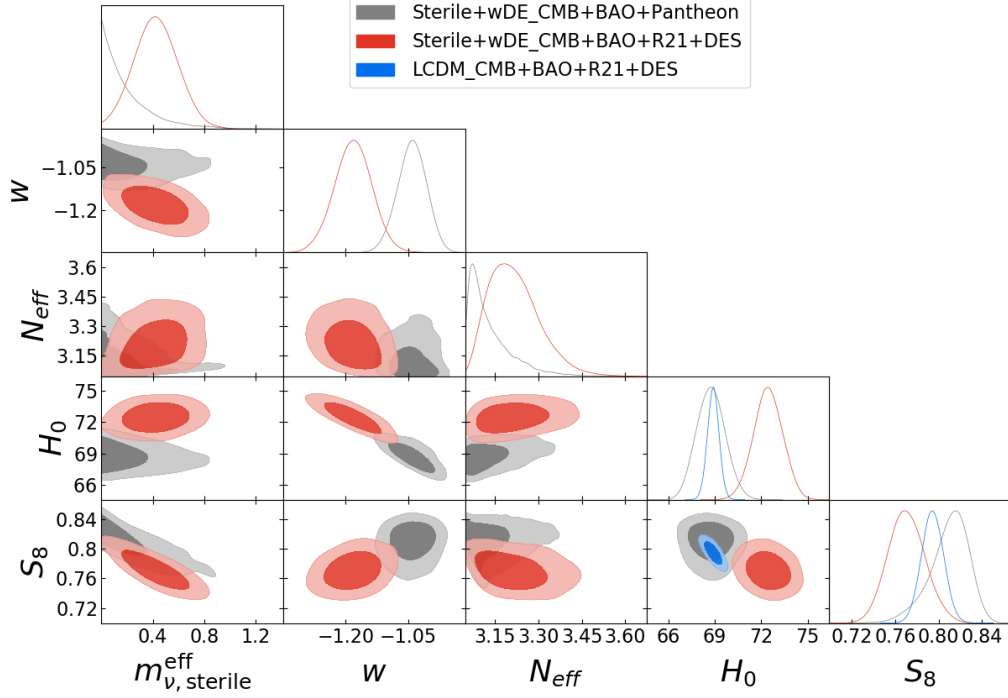


Figure 4: Posterior distributions of some parameters for the “ w Sterile” model. Different colors of grayish, reddish and bluish contours stand for different datasets.

D. ww_a Sterile

The 68% marginalized allowed ranges for the cosmological parameters in ww_a Sterile model are also summarized in Table IV. Two dimensional allowed regions and one dimensional posterior distributions are also depicted respectively in Figs. 6 and 7 respectively for the analysis including the R21 prior and the DES data simultaneously and separately.

Even when we take w and w_a as free parameters instead of Ω_K , the resultant H_0 and S_8 are almost same as those in the Ω_K Sterile model for datasets without the R21 prior. However, when we include the R21 prior and the DES data, a larger H_0 and a smaller S_8 are inferred, and interestingly, a more nonzero sterile neutrino mass of the order of sub-eV is indicated, even compared to that in the w Sterile model. This is due to the fact that a time-varying EoS has more degrees of freedom to change the distance to the last scattering surface whose effects are degenerate with those of N_{eff} and sterile neutrino masses. Finally, in Fig. 8, we show the redshift evolution of the dark energy equation of state w , considering the mean values of w_0 , w_a from the combined analysis \mathcal{D} +R21+DES. We observe a phantom

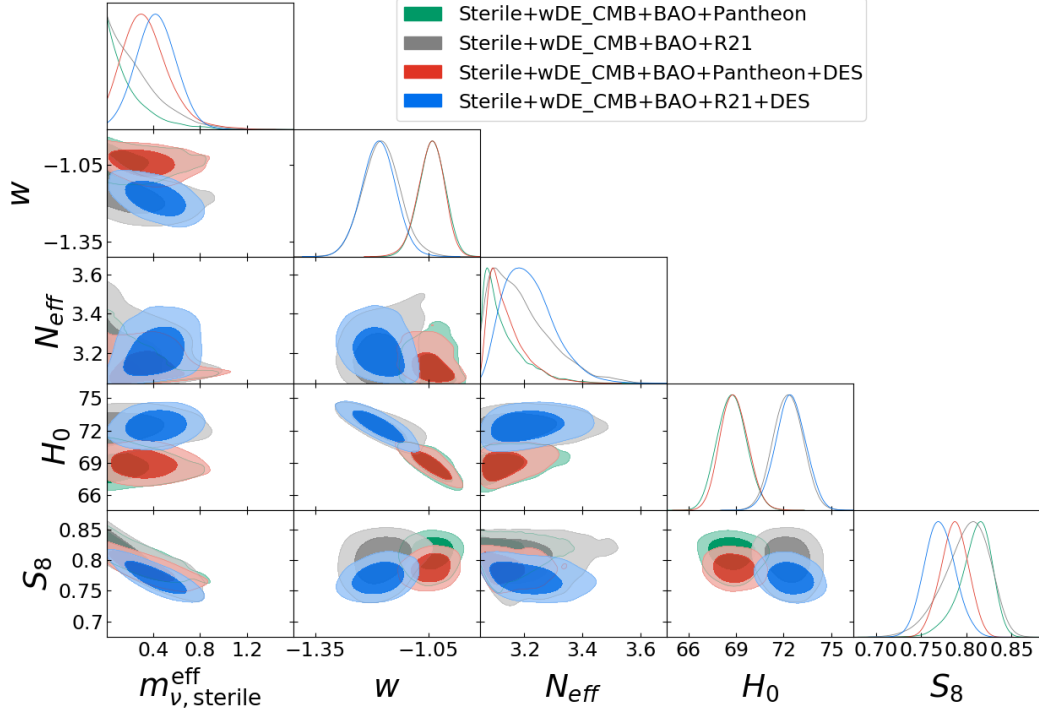


Figure 5: Posterior distributions of some parameters for the “ w Sterile” model. Different colors of greenish, grayish, reddish and bluish contours stand for different datasets.

nature of the dark energy ($w < -1$) in the high redshift, however, w is well consistent with the cosmological constant at the present epoch.

E. Comparison of the models

In this section we offer a comparison between various cosmological models with and without sterile neutrinos. To compare the goodness of fit in various cosmological models, in Table V we show the best-fit values of some key cosmological parameters, χ^2 for the best fit results and a model comparison statistics considering the datasets including the R21 prior and the DES data.

We focus on the best fit values of H_0 and S_8 obtained in different cosmological scenarios. When we include the R21 prior and the DES data, we find that the best fit values of H_0 in Sterile, Ω_K Sterile and w Sterile are quite similar ($H_0 \sim 70$ km/s/Mpc) but the best fit value of H_0 in ww_a Sterile models attains the maximum ($H_0 \sim 72.6$ km/s/Mpc). We note that the inclusion of the sterile neutrinos affects the expansion history a bit and such effects

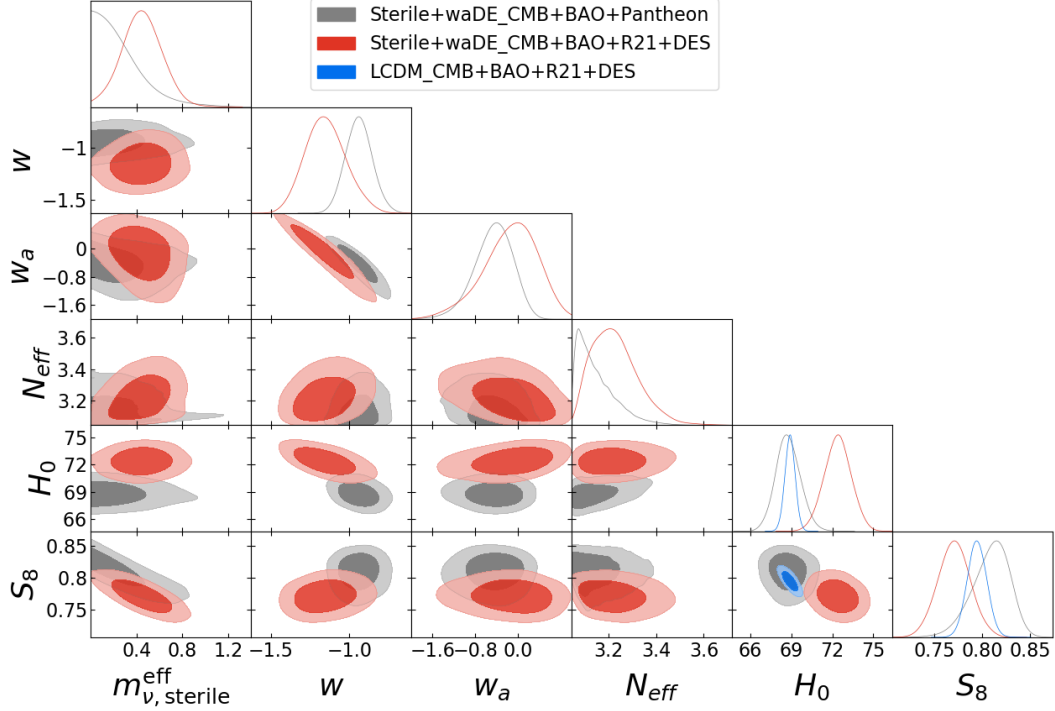


Figure 6: Posterior distributions of some parameters for “ ww_a Sterile” model. Different colors of grayish and reddish contours stand for different datasets. For comparison, that of Λ CDM model is also shown with bluish contour.

are clearly visible when we compare the models ww_a CDM and ww_a Sterile in the light of the H_0 tensions. On the other hand, focusing on the S_8 parameter, we find that S_8 attains the lowest best fit value in the ww_a Sterile model ($S_8 \sim 0.78$) compared to other models. Thus, we notice that among all the listed cosmological scenarios with and without the sterile neutrinos (see Table V), in the ww_a Sterile model H_0 attains the maximum value and S_8 attains the lowest value. In addition, we notice that χ^2_{Tot} for ww_a Sterile model attains the lowest value. This shows an improvement in the fit in the ww_a Sterile model for this combined dataset with R21 and DES.

We also perform a model comparison statistic, namely, the Akaike Information criteria (AIC) defined as [66, 67]: $\text{AIC} = \chi^2_{\text{Total}} + 2m$ (where m is the total number of free parameters of the model). At the end of Table V we show the values of ΔAIC calculated with respect to the reference model Λ CDM defined as $\Delta\text{AIC} = \text{AIC}(\text{Model}) - \text{AIC}(\Lambda\text{CDM})$. The negative value of ΔAIC indicates that the model is preferred over the Λ CDM model. According to the AIC analysis (see Table V) and the Jeffrey’s scale [68, 69], we see that the inclusion of

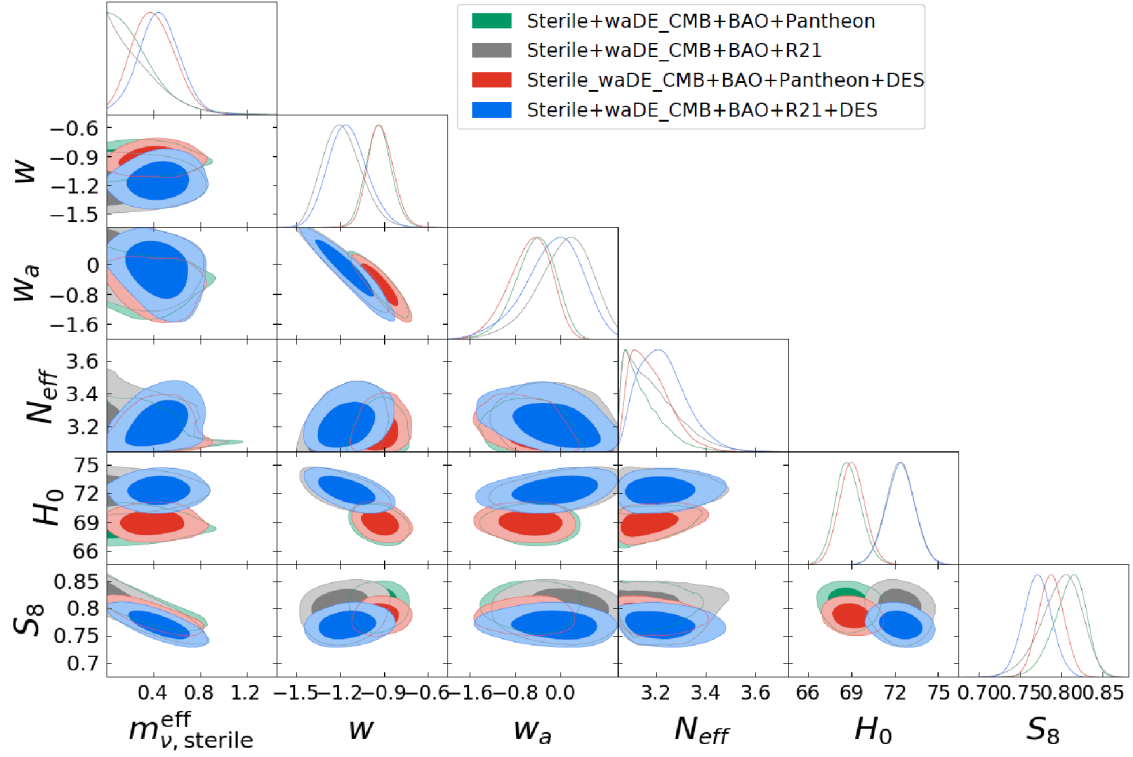


Figure 7: Posterior distributions of some parameters for “ ww_a Sterile” model. Different colors of greenish, grayish, reddish and bluish contours stand for different datasets.

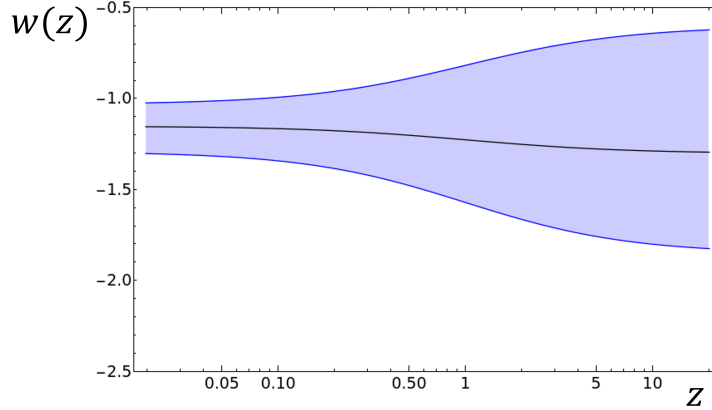


Figure 8: The evolution of w with respect to the red-shift z indicated by the dataset $\mathcal{D}+\mathbf{R21}+\mathbf{DES}$. The band and the median line correspond to those shown in Table III.

sterile neutrinos does not always offer a better fit compared to the models without sterile neutrinos. For example, although both w CDM and w Sterile are preferred over Λ CDM, but in the light of the AIC values, w CDM remains in the favored position compared to the w Sterile model. However, on the other hand, considering the dynamical DE equation of

Parameter	Λ CDM	w CDM	ww_a CDM	Sterile	Ω_K Sterile	w Sterile	ww_a Sterile
$m_{\nu, \text{sterile}}^{\text{eff}}$	—	—	—	0.05048	0.2068	0.017980	0.303472
N_{eff}	—	—	—	3.1974	3.1863	3.1822	3.1539
Ω_K	—	—	—	—	0.006193	—	—
w	—	-1.0163	-1.0398	—	—	-1.0232	-1.0636
w_a	—	—	-0.00353	—	—	—	-0.009172
H_0	68.90	69.32	69.77	69.30	70.16	70.05	72.5818
S_8	0.7970	0.7966	0.8035	0.7930	0.7818	0.80052	0.776137
χ_{CMB}^2	2771.46	2770.08	2767.20	2773.26	2772.22	2770.20	2770.64
χ_{BAO}^2	6.383	7.259	7.933	5.693	8.1259	7.2362	6.975
χ_{H0}^2	17.903	14.613	11.514	14.83	9.130	9.769	10.013
χ_{DES}^2	507.34	507.35	507.57	507.47	505.270	507.98	504.55
χ_{prior}^2	3.1933	3.249	4.974	3.694	3.443	3.625	2.932
χ_{Total}^2	3306.28	3302.55	3299.20	3304.95	3298.19	3298.80	3295.11
$\chi_{\text{Total}}^2 - \chi_{\text{Total}\Lambda\text{CDM}}^2$	—	-3.72	-7.08	-1.33	-8.09	-7.48	-11.17
ΔAIC	—	-1.72	-3.08	2.67	-2.09	-1.48	-3.17

Table V: The best-fit values of the cosmological parameters, χ_{Tot}^2 and the ΔAIC [= AIC (Model) – AIC (Λ CDM)] values for the datasets with R21 and DES (i.e. for the combined dataset \mathcal{D} +R21+DES).

state, our conclusion alters because according to the results, ww_a Sterile model gives better fit compared to ww_a CDM model (i.e. without sterile neutrinos). Although this improvement is very mild, but such improvement is likely due to the inclusion of the sterile neutrinos. This is not so surprising because an evidence of dynamical DE has been reported by DESI 2024 [70]. Therefore, we noticed that for this particular dataset, ww_a CDM model (with and without sterile neutrinos) state seems to be a very appealing candidate for further investigations. In fact, models with varying dark energy equation of state with or without the sterile neutrinos may offer new avenues in the light of the cosmological tensions.

To quantify how the tension is reduced in these models, we estimate and display the Gaussian tension for H_0 and S_8 in Table VI for the dataset \mathcal{D} +Pantheon, that means without

Parameter	Λ CDM	w CDM	ww_a CDM	Sterile	Ω_K Sterile	w Sterile	ww_a Sterile
H_0	67.74 ± 0.42	68.26 ± 0.82	68.32 ± 0.82	$67.89^{+0.40}_{-0.69}$	$68.25^{+0.68}_{-0.80}$	68.75 ± 0.92	$68.76^{+0.84}_{-0.93}$
σ_{H0}	4.95σ	3.81σ	3.76σ	4.57σ	3.95σ	3.28σ	3.32σ
S_8	$0.8234^{+0.0098}_{-0.011}$	0.827 ± 0.013	0.833 ± 0.014	$0.812^{+0.019}_{-0.014}$	$0.809^{+0.021}_{-0.014}$	$0.810^{+0.021}_{-0.013}$	$0.809^{+0.022}_{-0.016}$
σ_{S8}	2.38σ	2.38σ	2.59σ	1.51σ	1.34σ	1.40σ	1.29σ

Table VI: 68% limits of H_0 and S_8 , and the Gaussian tension for the H_0 tension and S_8 tension. To obtain this table, we use the dataset $\mathcal{D}+\text{Pantheon}$.

considering the R21 and DES data. The Gaussian tensions for H_0 and S_8 are respectively calculated as

$$\sigma_{H0} = \frac{H_0 \text{ Planck\&BAO\&Pantheon} - 73.30}{\sqrt{\sigma_{\text{Planck\&BAO\&Pantheon}}^2 + 1.04^2}}, \quad (3)$$

for the Hubble tension with direct measurement [2] and

$$\sigma_{S8} = \frac{S_8 \text{ Planck\&BAO\&Pantheon} - 0.776}{\sqrt{\sigma_{\text{Planck\&BAO\&Pantheon}}^2 + \frac{0.017^2 + 0.017^2}{2}}}, \quad (4)$$

for the S_8 tension with DES [16]. We find that in the Ω_K Sterile model, and ww_a Sterile model both H_0 tension and S_8 tension are reduced with a significance of over 1σ from Λ CDM model. In the w Sterile model, the H_0 tension is also reduced with a significance of over 1σ .² We again stress here that, in the ww_a Sterile model, the mass of sterile neutrino in sub-eV scale is preferred.

IV. SUMMARY AND CONCLUSIONS

In this paper, we have investigated constraints on the sterile neutrinos in the context of various cosmological scenarios in the light of the cosmological tensions such as the H_0 and S_8 tensions. When we do not include the data from R21 and DES, we only obtain an upper bound on $m_{\nu, \text{sterile}}^{\text{eff}}$ and N_{eff} is close to $N_{\text{eff}}^{\text{SM}}$ within 2σ in all models we considered in this paper, i.e., Λ CDM, Sterile, Ω_K Sterile, w Sterile and ww_a Sterile models. It should be noted

² We quote the 68% confidence limits $H_0 = 68.31 \pm 0.82$ and $S_8 = 0.829 \pm 0.011$ for ww_a model by $\mathcal{D}+\text{Pantheon}$ [1]. Therefore, we find that the relieve of the Hubble tension is mostly due to the introduction of w_a DE, while the relieve of the S_8 tension is due to the introduction of the sterile neutrino.

that, even in the presence of the sterile neutrinos, the spatial curvature in the Ω_K Sterile model is consistent with flat Universe within 1σ , the dark energy EoS is also consistent with $w = -1$.

However, when the DES data is included in the analysis, nonzero sterile neutrino masses is favored at 1σ level in Sterile, Ω_K Sterile, w Sterile models, and at 2σ in ww_a Sterile model. When the DES data and R21 are both included, we only obtain an upper bound on $m_{\nu, \text{sterile}}^{\text{eff}}$ at 2σ for Sterile, Ω_K Sterile, w Sterile models, while nonzero sterile neutrino masses are still favored at 2σ level in ww_a Sterile model. When R21 is included, the value of H_0 tends to be increased compared to that in the Λ CDM case in all extended models, and when the DES is included, S_8 decreases compared to the one without DES, and hence, in the ww_a Sterile model, nonzero sterile neutrino masses are inferred with the cosmological tensions being reduced to some extent.

It should also be mentioned that, in the presence of sterile neutrinos, negative spatial curvature of the Universe is favored at 2σ level when R21 and the DES data are included³. As we argued in this paper, the cosmological tensions can be reduced once we assume the existence of sterile neutrino in some extended frameworks such as nonflat Universe and a varying dark energy EoS model with nonzero sterile neutrino masses. This implies that the current cosmological data do not exclude the existence of sterile neutrinos, or even suggest its existence in some extended models.

ACKNOWLEDGMENTS

The authors thank the referee for some important comments. SP acknowledges the financial support from the Department of Science and Technology (DST), Govt. of India, under the Scheme ‘‘Fund for Improvement of S&T Infrastructure (FIST)’’ [File No. SR/FST/MS-I/2019/41]. This work was supported by JSPS KAKENHI Grant No. 19K03860, No. 19K03865, No. 23K03402 (OS), No. 19K03874, No. 23K17691 (TT), MEXT KAKENHI

³ One can indeed construct an inflationary model with $\Omega_K > 0$ [71, 72].

No. 23H04515 (TT), and JST SPRING, Grant No. JPMJSP2119 (YT).

- [1] N. Aghanim et al. (Planck), *Astron. Astrophys.* **641**, A6 (2020), [Erratum: *Astron. Astrophys.* 652, C4 (2021)], [arXiv:1807.06209 \[astro-ph.CO\]](#).
- [2] A. G. Riess et al., *Astrophys. J. Lett.* **934**, L7 (2022), [arXiv:2112.04510 \[astro-ph.CO\]](#).
- [3] W. L. Freedman, B. F. Madore, T. Hoyt, I. S. Jang, R. Beaton, M. G. Lee, A. Monson, J. Neeley, and J. Rich, *The Astrophysical Journal* **891**, 57 (2020), [arXiv:2002.01550 \[astro-ph.GA\]](#).
- [4] C. D. Huang, A. G. Riess, W. Yuan, L. M. Macri, N. L. Zakamska, S. Casertano, P. A. Whitelock, S. L. Hoffmann, A. V. Filippenko, and D. Scolnic, *The Astrophysical Journal* **889**, 5 (2020), [arXiv:1908.10883 \[astro-ph.CO\]](#).
- [5] D. W. Pesce et al., *Astrophys. J. Lett.* **891**, L1 (2020), [arXiv:2001.09213 \[astro-ph.CO\]](#).
- [6] K. C. Wong et al., *Mon. Not. Roy. Astron. Soc.* **498**, 1420 (2020), [arXiv:1907.04869 \[astro-ph.CO\]](#).
- [7] E. Di Valentino, O. Mena, S. Pan, L. Visinelli, W. Yang, A. Melchiorri, D. F. Mota, A. G. Riess, and J. Silk, *Class. Quant. Grav.* **38**, 153001 (2021), [arXiv:2103.01183 \[astro-ph.CO\]](#).
- [8] L. Perivolaropoulos and F. Skara, *New Astron. Rev.* **95**, 101659 (2022), [arXiv:2105.05208 \[astro-ph.CO\]](#).
- [9] N. Schöneberg, G. Franco Abellán, A. Pérez Sánchez, S. J. Witte, V. Poulin, and J. Lesgourgues, *Phys. Rept.* **984**, 1 (2022), [arXiv:2107.10291 \[astro-ph.CO\]](#).
- [10] E. Abdalla et al., *JHEAp* **34**, 49 (2022), [arXiv:2203.06142 \[astro-ph.CO\]](#).
- [11] M. Kamionkowski and A. G. Riess, *Ann. Rev. Nucl. Part. Sci.* **73**, 153 (2023), [arXiv:2211.04492 \[astro-ph.CO\]](#).
- [12] L. Verde, N. Schöneberg, and H. Gil-Marín, (2023), [arXiv:2311.13305 \[astro-ph.CO\]](#).
- [13] S. Joudaki et al., *Astron. Astrophys.* **638**, L1 (2020), [arXiv:1906.09262 \[astro-ph.CO\]](#).
- [14] A. Amon et al. (DES), *Phys. Rev. D* **105**, 023514 (2022), [arXiv:2105.13543 \[astro-ph.CO\]](#).
- [15] L. F. Secco et al. (DES), *Phys. Rev. D* **105**, 023515 (2022), [arXiv:2105.13544 \[astro-ph.CO\]](#).
- [16] T. M. C. Abbott et al. (DES), *Phys. Rev. D* **105**, 023520 (2022), [arXiv:2105.13549 \[astro-ph.CO\]](#).

- [17] A. Loureiro et al. (KiDS, Euclid), *Astron. Astrophys.* **665**, A56 (2022), [arXiv:2110.06947 \[astro-ph.CO\]](#).
- [18] H. Miyatake et al., *Phys. Rev. D* **108**, 123517 (2023), [arXiv:2304.00704 \[astro-ph.CO\]](#).
- [19] S. Sugiyama et al., *Phys. Rev. D* **108**, 123521 (2023), [arXiv:2304.00705 \[astro-ph.CO\]](#).
- [20] T. Sunayama et al., (2023), [arXiv:2309.13025 \[astro-ph.CO\]](#).
- [21] S. Schael et al. (ALEPH, DELPHI, L3, OPAL, SLD, LEP Electroweak Working Group, SLD Electroweak Group, SLD Heavy Flavour Group), *Phys. Rept.* **427**, 257 (2006), [arXiv:hep-ex/0509008](#).
- [22] M. G. Aartsen et al. (IceCube), *Phys. Rev. Lett.* **125**, 141801 (2020), [arXiv:2005.12942 \[hep-ex\]](#).
- [23] K. Abe et al. (Super-Kamiokande), *Phys. Rev. D* **94**, 052010 (2016), [arXiv:1606.07538 \[hep-ex\]](#).
- [24] A. Gando et al. (KamLAND), *Phys. Rev. D* **88**, 033001 (2013), [arXiv:1303.4667 \[hep-ex\]](#).
- [25] S. Gariazzo, C. Giunti, and M. Laveder, *JHEP* **11**, 211 (2013), [arXiv:1309.3192 \[hep-ph\]](#).
- [26] M. Archidiacono, N. Fornengo, S. Gariazzo, C. Giunti, S. Hannestad, and M. Laveder, *JCAP* **06**, 031 (2014), [arXiv:1404.1794 \[astro-ph.CO\]](#).
- [27] S. Gariazzo, C. Giunti, and M. Laveder, *JCAP* **04**, 023 (2015), [arXiv:1412.7405 \[astro-ph.CO\]](#).
- [28] S. Roy Choudhury and S. Choubey, *Eur. Phys. J. C* **79**, 557 (2019), [arXiv:1807.10294 \[astro-ph.CO\]](#).
- [29] S. Hagstotz, P. F. de Salas, S. Gariazzo, M. Gerbino, M. Lattanzi, S. Vagnozzi, K. Freese, and S. Pastor, *Phys. Rev. D* **104**, 123524 (2021), [arXiv:2003.02289 \[astro-ph.CO\]](#).
- [30] M. Archidiacono, S. Gariazzo, C. Giunti, S. Hannestad, and T. Tram, *JCAP* **12**, 029 (2020), [arXiv:2006.12885 \[astro-ph.CO\]](#).
- [31] E. Di Valentino, S. Gariazzo, C. Giunti, O. Mena, S. Pan, and W. Yang, *Phys. Rev. D* **105**, 103511 (2022), [arXiv:2110.03990 \[astro-ph.CO\]](#).
- [32] Z. Sakr, *Universe* **8**, 284 (2022).
- [33] M. Maltoni, T. Schwetz, M. A. Tortola, and J. W. F. Valle, *Nucl. Phys. B* **643**, 321 (2002), [arXiv:hep-ph/0207157](#).
- [34] P. Adamson et al. (Daya Bay, MINOS), *Phys. Rev. Lett.* **117**, 151801 (2016), [Addendum: *Phys.Rev.Lett.* 117, 209901 (2016)], [arXiv:1607.01177 \[hep-ex\]](#).
- [35] J. M. Berryman, P. Coloma, P. Huber, T. Schwetz, and A. Zhou, *JHEP* **02**, 055 (2022), [arXiv:2111.12530 \[hep-ph\]](#).

- [36] J. Hamann, S. Hannestad, G. G. Raffelt, and Y. Y. Y. Wong, *JCAP* **09**, 034 (2011), [arXiv:1108.4136 \[astro-ph.CO\]](#).
- [37] P. Di Bari, *Phys. Rev. D* **65**, 043509 (2002), [arXiv:hep-ph/0108182](#).
- [38] V. Barger, J. P. Kneller, H.-S. Lee, D. Marfatia, and G. Steigman, *Phys. Lett. B* **566**, 8 (2003), [arXiv:hep-ph/0305075](#).
- [39] A. D. Dolgov and F. L. Villante, *Nucl. Phys. B* **679**, 261 (2004), [arXiv:hep-ph/0308083](#).
- [40] O. Seto and Y. Toda, *Phys. Rev. D* **104**, 063019 (2021), [arXiv:2104.04381 \[astro-ph.CO\]](#).
- [41] N. Saviano, A. Mirizzi, O. Pisanti, P. D. Serpico, G. Mangano, and G. Miele, *Phys. Rev. D* **87**, 073006 (2013), [arXiv:1302.1200 \[astro-ph.CO\]](#).
- [42] J. R. Kristiansen and O. Elgaroy, *Astron. Astrophys.* **532**, A67 (2011), [arXiv:1104.0704 \[astro-ph.CO\]](#).
- [43] H. Motohashi, A. A. Starobinsky, and J. Yokoyama, *Prog. Theor. Phys.* **124**, 541 (2010), [arXiv:1005.1171 \[astro-ph.CO\]](#).
- [44] E. Di Valentino, A. Melchiorri, and J. Silk, *Nature Astron.* **4**, 196 (2019), [arXiv:1911.02087 \[astro-ph.CO\]](#).
- [45] W. Handley, *Phys. Rev. D* **103**, L041301 (2021), [arXiv:1908.09139 \[astro-ph.CO\]](#).
- [46] T. Sekiguchi and T. Takahashi, *Phys. Rev. D* **103**, 083507 (2021), [arXiv:2007.03381 \[astro-ph.CO\]](#).
- [47] O. Seto and Y. Toda, *Phys. Rev. D* **107**, 083512 (2023), [arXiv:2206.13209 \[astro-ph.CO\]](#).
- [48] T. Sekiguchi and T. Takahashi, *Phys. Rev. D* **103**, 083516 (2021), [arXiv:2011.14481 \[astro-ph.CO\]](#).
- [49] M. Chevallier and D. Polarski, *Int. J. Mod. Phys. D* **10**, 213 (2001), [arXiv:gr-qc/0009008](#).
- [50] E. V. Linder, *Phys. Rev. Lett.* **90**, 091301 (2003), [arXiv:astro-ph/0208512](#).
- [51] R. E. Keeley, S. Joudaki, M. Kaplinghat, and D. Kirkby, *JCAP* **12**, 035 (2019), [arXiv:1905.10198 \[astro-ph.CO\]](#).
- [52] T. M. C. Abbott et al. (DES), *Phys. Rev. D* **98**, 043526 (2018), [arXiv:1708.01530 \[astro-ph.CO\]](#).
- [53] P. A. R. Ade et al. (Planck), *Astron. Astrophys.* **571**, A16 (2014), [arXiv:1303.5076 \[astro-ph.CO\]](#).
- [54] N. Aghanim et al. (Planck), *Astron. Astrophys.* **641**, A5 (2020), [arXiv:1907.12875 \[astro-ph.CO\]](#).

- [55] N. Aghanim et al. (Planck), *Astron. Astrophys.* **641**, A8 (2020), [arXiv:1807.06210 \[astro-ph.CO\]](#).
- [56] F. Beutler, C. Blake, M. Colless, D. Jones, L. Staveley-Smith, L. Campbell, Q. Parker, W. Saunders, and F. Watson, *Mon. Not. Roy. Astron. Soc.* **416**, 3017 (2011), [arXiv:1106.3366 \[astro-ph.CO\]](#).
- [57] A. J. Ross, L. Samushia, C. Howlett, W. J. Percival, A. Burden, and M. Manera, *Mon. Not. Roy. Astron. Soc.* **449**, 835 (2015), [arXiv:1409.3242 \[astro-ph.CO\]](#).
- [58] S. Alam et al. (BOSS), *Mon. Not. Roy. Astron. Soc.* **470**, 2617 (2017), [arXiv:1607.03155 \[astro-ph.CO\]](#).
- [59] D. M. Scolnic et al. (Pan-STARRS1), *Astrophys. J.* **859**, 101 (2018), [arXiv:1710.00845 \[astro-ph.CO\]](#).
- [60] <http://des.ncsa.illinois.edu/releases/y1a1/key-products>.
- [61] A. Lewis and S. Bridle, *Phys. Rev. D* **66**, 103511 (2002), [arXiv:astro-ph/0205436](#).
- [62] A. Gelman and D. B. Rubin, *Statist. Sci.* **7**, 457 (1992).
- [63] S. Dhawan, D. Brout, D. Scolnic, A. Goobar, A. G. Riess, and V. Miranda, *Astrophys. J.* **894**, 54 (2020), [arXiv:2001.09260 \[astro-ph.CO\]](#).
- [64] S. Dodelson, A. Melchiorri, and A. Slosar, *Phys. Rev. Lett.* **97**, 041301 (2006), [arXiv:astro-ph/0511500](#).
- [65] O. Seto and Y. Toda, *Phys. Rev. D* **103**, 123501 (2021), [arXiv:2101.03740 \[astro-ph.CO\]](#).
- [66] H. Akaike, *IEEE Transactions on Automatic Control* **19**, 716 (1974).
- [67] A. R. Liddle, *Mon. Not. Roy. Astron. Soc.* **377**, L74 (2007), [arXiv:astro-ph/0701113](#).
- [68] H. Jeffreys, *The Theory of Probability*, 3rd ed. (Oxford University Press, 1961).
- [69] R. E. Kass and A. E. Raftery, *J. Am. Statist. Assoc.* **90**, 773 (1995).
- [70] K. Lodha et al. (DESI), (2024), [arXiv:2405.13588 \[astro-ph.CO\]](#).
- [71] A. D. Linde, *Phys. Rev. D* **59**, 023503 (1999), [arXiv:hep-ph/9807493](#).
- [72] A. D. Linde, M. Sasaki, and T. Tanaka, *Phys. Rev. D* **59**, 123522 (1999), [arXiv:astro-ph/9901135](#).